ACS APPLIED MATERIALS & INTERFACES

Research Article

www.acsami.org

Polystyrene Nanofiber Materials Modified with an Externally Bound Porphyrin Photosensitizer

Petr Henke,[†] Kamil Lang,[‡] Pavel Kubát,*[,§] Jan Sýkora,[§] Miroslav Šlouf,[⊥] and Jiří Mosinger*[,†,‡]

[†]Faculty of Science, Charles University in Prague, Hlavova 2030, 128 43 Praha 2, Czech Republic

[‡]Institute of Inorganic Chemistry, v.v.i., Academy of Sciences of the Czech Republic, Husinec-Řež 1001, 250 68 Řež, Czech Republic

[§]J. Heyrovský Institute of Physical Chemistry, v.v.i, Academy of Sciences of the Czech Republic, Dolejškova 3, 182 23 Praha 8, Czech Republic

[⊥]Institute of Macromolecular Chemistry, v.v.i., Academy of Sciences of the Czech Republic, Heyrovsky Sq. 2, 162 06 Praha 6, Czech Republic

Supporting Information

ABSTRACT: Polystyrene ion-exchange nanofiber materials with large surface areas and adsorption capacities were prepared by electrospinning followed by the sulfonation and adsorption of a cationic 5,10,15,20-tetrakis(1-methylpyridinium-4-yl)porphyrin (TMPyP) photosensitizer on the nanofiber surfaces. The morphology, structure, and photophysical properties of these nanofiber materials were characterized by microscopic methods and steady-state and time-resolved fluorescence and absorption spectroscopies. The externally bound TMPyP can be excited by visible light to form triplet states and singlet oxygen $O_2(^1\Delta_g)$ and singlet oxygen-sensitized delayed fluorescence (SODF). The photophysical properties of the nanofibers were strongly dependent on the amount of bound TMPyP molecules and their organization on the nanofiber surfaces. The nanofibers demonstrated photooxidative activity toward inorganic and organic molecules and antibacterial activity against *E. coli* due to the sensitized formation of $O_2(^1\Delta_g)$ that is an effective oxidation/cytotoxic agent. The nanofiber materials also adsorbed heavy metal cations (Pb^{2+}) and removed them from the water environment.

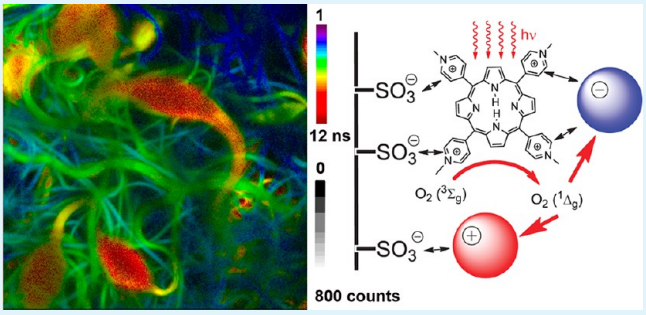

KEYWORDS: *nanofiber, porphyrin, singlet oxygen, adsorption, photooxidation, antibacterial*

1. INTRODUCTION

The overuse of antibiotics has allowed many pathogens to develop resistances to these drugs. Alternative way to kill bacteria not involving antibiotics is antimicrobial photodynamic therapy (PDT).[1,2] PDT is a well-known technique for the targeted destruction of cells, and it is typically used for tumor therapy.[3] In PDT, light is used to activate photosensitizer molecules, creating singlet oxygen, $O_2(^1\Delta_g)$, and other reactive oxygen species that kill the surrounding cells.[4,5]

We recently developed nanofiber materials doped with porphyrins that generate high yields of $O_2(^1\Delta_g)$ upon visible light irradiation, which efficiently kills bacteria[6,7] and viruses.[8] These low-cost electrospun materials, which are composed of fibers with diameters ranging from tens of nanometers to a few micrometers, were characterized by large surface areas and porous structures[9,10] and prevented the passage of bacteria and other particles by detaining them on the surface. The small diameters of the nanofibers allow for the diffusion of $O_2(^1\Delta_g)$ outside of the fibers, where it photooxidizes biological targets, e.g., cell membranes[11] or proteins inside the cells.[12] Because of their simplicity and biological compatibility, it is possible to use these nanofiber materials in medical applications, such as for the treatment of infected wounds in patients,[13] which is usually time-consuming and costly. Photosensitizers that are encapsulated in the nanofiber materials do not penetrate the surface of the skin or wound and cannot harm healthy human cells.

A critical aspect of the materials with a photosensitizer immobilized inside fibers is diffusion length of $O_2(^1\Delta_g)$ (typically tens to hundreds of nanometers),[14] which limits photooxidation processes to areas in close proximity to the fiber surfaces. Higher photooxidation efficiency requires the organization of photosensitizer molecules near fiber surfaces, which is not easy to control,[15] and/or postprocessing of the hydrophobic polymeric surface, which may damage the nanofibers.

In this paper, we describe the fabrication and properties of polystyrene nanofiber materials with a cationic 5,10,15,20-tetrakis(1-methylpyridinium-4-yl)porphyrin photosensitizer (TMPyP, whose quantum yield of $O_2(^1\Delta_g)$ formation in water is 0.74)[16] externally bound to negatively charged

Received: January 30, 2013
Accepted: April 8, 2013
Published: April 8, 2013

   dx.doi.org/10.1021/am4004057 | ACS Appl. Mater. Interfaces 2013, 5, 3776−3783

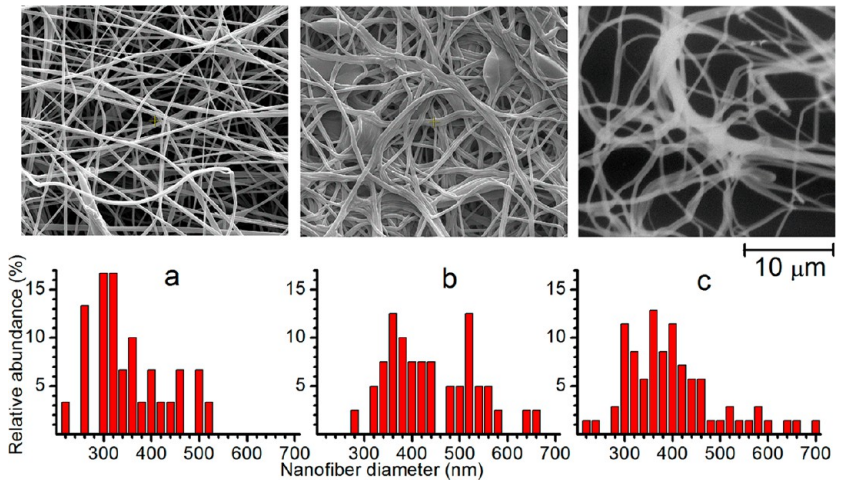

Figure 1. SEM images of the dry electrospun nanofiber material (a) before and (b) after 10 min of sulfonation, and (c) the sulfonated nanofiber material immersed in H_2O. The images are accompanied by the corresponding diameter distributions.

nanofiber surfaces. We propose two applications for these materials: (i) the oxidative degradation of surrounding species by reactions with photoproduced $O_2(^1\Delta_g)$ and (ii) the removal of positively charged species from the environment by adsorption.

2. EXPERIMENTAL SECTION

Chemicals. The following chemicals were purchased from Sigma-Aldrich and used as received: 5,10,15,20-tetrakis(1-methylpyridinium-4-yl)porphyrin tetra (*p*-toluenesulfonate) (TMPyP), uric acid, *N,N*-dimethyl formamide (DMF), limonene, tetraethylammonium bromide (TEAB), LB agar, ampicillin sodium, chlorosulfonic acid (HSO_3Cl), potassium iodide and lead(II) nitrate. A Pb standard (1000 mg/L) for atomic absorption spectroscopy was purchased from Merck. The reagents 5-bromo-4-chloro-3-indolyl-*β*-D-galactopyranoside (X-Gal) and isopropyl-*β*-D-thiogalactoside (IPTG) were used as received from Invitrogen, USA. Polystyrene Krasten 137 was purchased from Synthos Kralupy a.s., Czech Republic.

Electrospinning. A mixture of 0.07 wt % TEAB and 99.93 wt % polystyrene was dissolved in DMF/limonene (1:2 w/w) to prepare a 17% solution for the fabrication of polystyrene nanofiber materials. The nanofiber materials were produced using the Nanospider electrospinning industrial technology.[6]

Sulfonation. Electrospun polystyrene nanofiber material was fixed on quartz substrates and immersed in chlorosulfonic acid at 10−12 °C for 1−20 min.[17] Finally, the materials were washed with deionized water until the pH value reached 6−7 and stored in water.

Ion Exchange Capacity (IEC). IEC of the sulfonated materials was determined by titration. Approximately 45 cm^2 of the material were treated with 20 mL of 10 mM NaOH solution for 1 day to completely replace H^+ with Na^+. The remaining NaOH was titrated potentiometrically with 10 mM HCl. The IECs were related to the mass of the dried materials.

Ion Exchange with TMPyP. The sulfonated polystyrene nanofiber material (3 cm^2, IEC = 4 mmol g^{-1}) was immersed in 9 mL of a solution of TMPyP in deionized water for 10 min. The concentrations of TMPyP were 10^{-5}, 10^{-4}, and 10^{-2} M for low, medium, and high loading of TMPyP, respectively.

Scanning Electron Microscopy (SEM). The nanofiber morphology was studied with a scanning electron Quanta 200 FEG microscope (FEI, Czech Republic). Dry fibers were covered with a 4 nm layer of Pt and observed using a secondary electron detector at high vacuum. Wet fibers were observed in the presence of water (sample temperature +1 °C, chamber pressure 400−700 Pa) using ESEM and/or wet-STEM detectors as in our previous work.[18] The thickness of the nanofibers was estimated by means of NIS Elements 4.0 image analysis software (Laboratory Imaging, Czech Republic).

Confocal Fluorescence and Fluorescence Lifetime Imaging Microscopy. These measurements were carried out using a MicroTime 200 inverted epifluorescence confocal microscope (PicoQuant, Germany). The experimental configuration included a pulsed diode laser (LDH−P-C-405, 405 nm, PicoQuant) providing 80 ps pulses at a frequency of 40 MHz, a 505DRLP dichroic mirror, an LP500 long-pass filter (Omega Optical), a water immersion objective (1.2 NA, 60×, Olympus), and a SPAD detector (Perkin-Elmer, Canada).

Atomic Absorption Spectroscopy (AAS). AAS was performed using a model AAS3 Carl Zeiss spectrometer (Jena, Germany) and used for determining Pb^{2+} concentrations.

Fourier Transform Infrared Spectra (FTIR). FTIR were collected in the transmission mode using a Thermo Scientific FTIR spectrometer (Nicolet 6700) with Happ-Genzel apodization in the 400 − 4000 cm^{-1} range.

UV/vis Absorption and Luminescence Spectroscopy. The UV/vis absorption spectra were recorded using Unicam 340 and Varian 4000 spectrometers. The luminescence spectra were monitored on a Fluorolog 3 spectrometer equipped with a cooled TBX-05-C photon detection module (Horiba Jobin Yvon) or with a Hamamatsu H10330−45 photomultiplier for measurement of the $O_2(^1\Delta_g)$ emission spectra. Fluorescence lifetime measurements were performed with a Fluorolog 3 spectrometer using a laser-diode excitation at 405 nm (NanoLED-405LH, pulse width 750 ps, 1 MHz) and a cooled TBX-05-C photon detection module in a time-correlated single-photon counting regime. The decay curves were fitted to exponential functions using the iterative reconvolution procedure of the DAS6 software (v. 6.4, Horiba Jobin Yvon, 2009).

Time-Resolved near-Infrared Phosphorescence of $O_2(^1\Delta_g)$ at 1270 nm was monitored using a Ge detector (Judson J16−8SP-R05M-HS) with excitation by a Lambda Physik Compex 102 excimer laser (λ_{exc} = 308 nm) or an F3002 dye laser (λ_{exc} = 425 nm). The short-lived signal produced by the scattering of laser pulses and/or porphyrin fluorescence was eliminated by subtracting the signal in argon-saturated solution from the signal recorded in air-saturated aqueous solution. The signal-to-noise ratio was improved by averaging 1000 individual traces.

Triplet States and Singlet Oxygen-Sensitized Delayed Fluorescence (SODF). Triplet states and SODF were recorded using an LKS 20 kinetic spectrometer (Applied Photophysics, UK). The samples were excited with the same lasers that were used for the phosphorescence measurements. The triplet states of TMPyP were monitored in both transmission and diffuse reflectance modes. The kinetics of the triplet states were probed at 480 nm using a 250 W Xe lamp equipped with a pulse unit and an R928 photomultiplier. The fluorescence time profiles were recorded at 650 nm. The SODF was

calculated from the difference between the fluorescence of TMPyP in air- and argon-saturated solutions.

Photooxidation of Model Species by Nanofiber Materials. A piece of the TMPyP nanofiber material was placed in a thermostatted 10 mm quartz cell (22 °C) containing iodide solution.[19] The cell was irradiated with visible light (λ > 400 nm) from a stabilized xenon lamp (300 or 500 W, Newport). The UV/vis absorbance changes at 351 nm, attributed to the formation of I_3^-, were recorded at regular intervals and compared to a blank solution of the same composition that was stored in the dark. The decrease of the uric acid concentration with irradiation time was observed at the absorption maximum of 291 nm.

Antibacterial tests. The TMPyP nanofiber materials were placed on bacterial agar plates. Then, the surfaces of the materials were enriched with 20 μL X-Gal (20 mg/mL in 50% DMF) and 20 μL IPTG (23 mg/mL) and then inoculated with 20 μL (700 CFU) of a suspension of *Escherichia coli* DH5α (Invitrogen, CA, USA) containing the pGEM11Z plasmid (Promega WI, USA), which produces β-galactosidase. The agar plates were either illuminated with white light from a 400 W solar daylight simulator (Sol1A Newport, USA) for 2 min or stored in the dark. The plates were incubated overnight in darkness at 37 °C to allow the individual bacteria to grow and form visible blue-green colonies. The blue-green color of the colonies was due to an indolyl dye produced from the X-Gal substrate by bacterial β-galactosidase.

3. RESULTS AND DISCUSSION

Preparation and Morphology of the Nanofiber Materials. The structure of the original electrospun polystyrene nanofiber materials was visualized by SEM (Figure 1a). Sulfonation of the original electrospun nanofiber materials using HSO_3Cl led to the formation of cation exchange functionality on the nanofiber surfaces. The ion exchange capacity (IEC) depended upon the sulfonation time, with a maximum value of 4 mmol g^{-1} (Figure 2a).

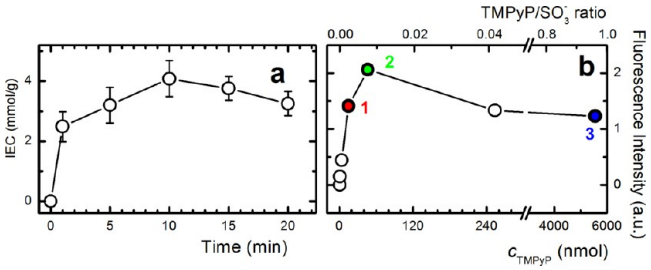

Figure 2. (a) IEC of the nanofiber materials with different sulfonation times. (b) Fluorescence intensity as a function of adsorbed TMPyP on the sulfonated nanofibers for low (2.5×10^{-3}, label 1), medium (7.5×10^{-3}, label 2), and high (0.93, label 3) TMPyP/SO_3^- molar ratios, the materials were excited at 430 nm).

Sulfonation was accompanied by the slight increase of the nanofiber diameters (Figure 1b, c). The nanofibrous character of the materials was not changed by this treatment (Figure 1b) or by long-term storage in water (Figure 1c). This behavior was different from behavior described previously for fibers prepared by electrospinning sulfonated polystyrene (IEC ≈ 4.8 mmol g^{-1}), which were moisture sensitive and tended to lose their fibrous structure when exposed to water or even humid air.[20] At high IEC, access to the sulfonic groups may be restricted by steric hindrance due to the small pore sizes and Coulombic repulsive forces between negatively charged sulfonic groups. Longer sulfonation times most likely introduced sulfone bridges and other cross-links into the fibers and decreased the IEC.

The sulfonated nanofiber material (IEC = 4 mmol g^{-1}) was used as a substrate for the adsorption of the cationic photosensitizer TMPyP and the preparation of the photoactive TMPyP-modified nanofiber materials (Figure 3). The TMPyP molecule has four positively charged methylpyridyl groups that may saturate from one to four binding sites on the nanofiber surface. For photophysical/photochemical experiments, we prepared three samples with low, medium, and high loadings that corresponded to TMPyP/SO_3^- molar ratios of 2.5×10^{-3}, 7.5×10^{-3}, and 0.93, respectively, by ion exchange from solutions of TMPyP in deionized water (Figure 2b). The adsorption of TMPyP from aqueous solution was monitored quantitatively by observing the disappearance of the Soret and Q bands from the UV/vis spectra of the water phase (see the Supporting Information, Figure S1).

FTIR Spectra. The chemical composition of the polystyrene nanofiber materials was confirmed by FTIR spectroscopy. The main absorption bands of the original electrospun material (Figure 4a) were observed at 1600, 1492, and 1451 cm^{-1} (C=C aromatic stretching) and 1028 cm^{-1} (C−H in-plane bending). The sulfonation reaction produced a strong band at 1036 cm^{-1} and a doublet (at approximately 1210 and 1160 cm^{-1}), which correspond to the symmetric and asymmetric SO_2 stretching vibrations, respectively (Figure 4b).[21] Sulfonation proceeds easily for the phenyls, even though the dissociation energy of the C−H bond is higher in aromatic (~430 kJ/mol) than in aliphatic (~ 380 kJ/mol) compounds. The appearance of characteristic bands assigned to the in-plane bending of the para-substituted phenyl ring at 1127 and 1006 cm^{-1} confirms the success of nanofiber sulfonation. The narrow band from the deformation vibration of the *N*-methylpyridinium group[22] at 1638 cm^{-1} dominated the FTIR spectra of the TMPyP nanofiber materials (Figure 4c). Other deformation and stretching vibrations of the *N*-methylpyridinium and N^+-CH_3 groups at approximately 1200 cm^{-1} (lit.[23]) overlapped the strong absorption by the $-SO_3^-$ group.

UV−Vis Absorption and Fluorescence Spectra. Figure 5A shows the UV/vis spectra of the TMPyP nanofiber materials. The spectra are characterized by the Soret band and four Q absorption bands that are typical of the D_{2h} molecular symmetry of TMPyP (Figure 3c). The Soret band was red-shifted by 7 nm, i.e., from 423 nm for TMPyP in aqueous solution to 430 nm for TMPyP bound to nanofibers.

The fluorescence spectra of TMPyP changed significantly upon binding to the sulfonated nanofiber material (Figure 5B). The data from the literature report changes in the fluorescence spectrum of TMPyP that are induced by the polarity of the environment (solvent).[24,25] Band broadening masks the vibrational structure in the fluorescence spectrum of TMPyP in aqueous solution. One explanation for this band broadening effect involves the mixing of the S_1 state with a nearby charge-transfer state mediated by the vibrational motion of the *N*-methylpyridinium groups.[26] Recent DFT calculations revealed changes in the electron density distribution of TMPyP after excitation into the excited S_1 and S_2 states.[27] The electron density is partially transferred from the central porphyrin ring to the methylpyridinium peripheral substituents. In less polar environments (e.g., in methanol), the excited states are destabilized and fluorescence spectrum exhibits a vibronic resolution.

Our results showed that the adsorption of TMPyP molecules from aqueous solution started preferentially with the multiple binding of TMPyP to a few $-SO_3^-$ groups, where most

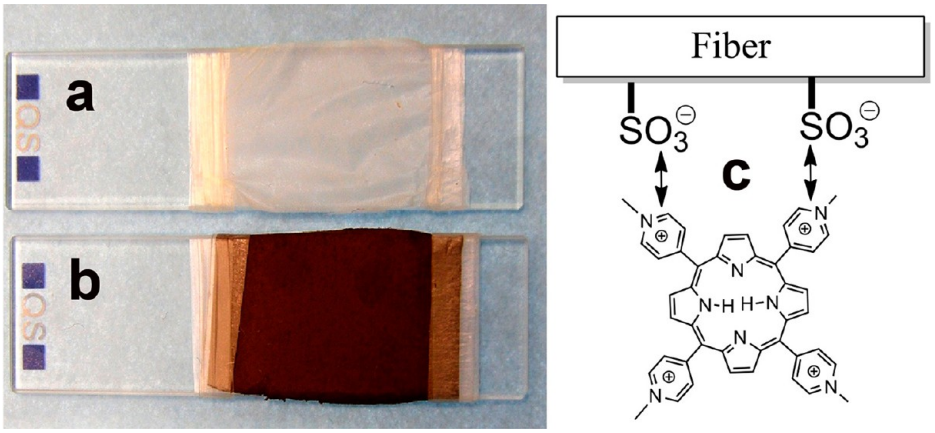

Figure 3. Images of the sulfonated nanofiber materials on a quartz plate (a) before and (b) after adsorption of cationic TMPyP (high loading, $TMPyP/SO_3^-$ = 0.93). (c) Schematic structure of TMPyP bound to the sulfonated nanofiber.

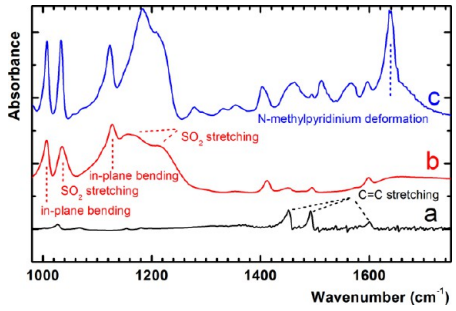

Figure 4. (a) FTIR spectra of the original electrospun nanofiber material, (b) the sulfonated material, and (c) material after adsorption of TMPyP (high loading, $TMPyP/SO_3^-$ = 0.93). Data are offset for better clarity.

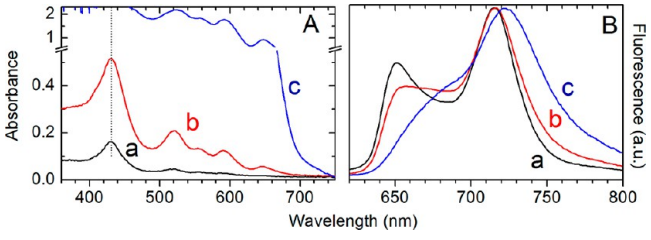

Figure 5. (A) Absorption and (B) normalized fluorescence (excited at 430 nm) spectra of the TMPyP nanofiber material immersed in water for (a) low ($TMPyP/SO_3^-$ = 2.5 × 10^{-3}), (b) medium ($TMPyP/SO_3^-$ = 7.5 × 10^{-3}), and (c) high ($TMPyP/SO_3^-$ = 0.93) loadings of TMPyP.

porphyrin units were parallel/nearly parallel to the nanofiber surface. Thus, the contact between water molecules and porphyrin rings located near the surface was limited, and the effect of a less polar environment was accompanied by well-resolved fluorescence bands (Figure 5B, a). At high loading, the TMPyP molecules can be attached to the surface by only one *N*-methylpyridinium group and the porphyrin rings are inclined or perpendicular to the surface. Orientation toward more polar environments is indicated by the unresolved fluorescence bands (Figure 5B, c). The fluorescence spectra of the dry TMPyP nanofiber materials or the materials after 70 days of aging showed slow reorganization of the TMPyP molecules with a slight formation of aggregates, which was indicated by the appearance of a new broad emission band at 620 nm (see the Supporting Information, Figure S7).

The averages of TMPyP fluorescence lifetimes, measured at the maxima of the Q bands, were considerably shorter at high TMPyP loading levels (see the Supporting Information, Table S2) because of self-quenching and orientation of the porphyrin rings toward the water environment. The extremely long average lifetime of 11.3 ns measured for the surface with the low loading (molar ratio $TMPyP/SO_3^-$ = 2.5 × 10^{-3}) confirmed the less polar character of the environment of the porphyrin rings.

Fluorescence Lifetime Imaging Microscopy (FLIM). The kinetics and intensity of the TMPyP fluorescence were monitored with FLIM at different sites on the TMPyP nanofiber material for the three TMPyP loadings. To evaluate fluorescence decays recorded for each pixel, the average lifetimes were calculated from $\tau_{av} = \Sigma I_i t_i / \Sigma I_i$, where I_i and t_i are the intensity and time corresponding to the i-th channel in the time-correlated single photon counting histogram, respectively. Lifetime images are displayed using a continuous pseudocolor scale (from blue to red), where each color represents an average fluorescence lifetime of TMPyP.

The fluorescence intensity images (Figure 6a, d) confirmed the SEM results that the nanofibrous structure of the original electrospun material was not significantly affected by sulfonation and TMPyP adsorption. The average lifetimes of TMPyP at the high loading ranged between 2.3 and 5 ns (Figure 6c) and indicate orientation of porphyrins toward polar aqueous environment (see above). These lifetimes were shorter than the fluorescence lifetime of TMPyP in aqueous solution (~ 5 ns).[25] Although the stacking strength of TMPyP is low,[28] the behavior of TMPyP on the nanofiber material tends to be complicated by aggregate formation and fluorescence self-quenching.

The lower loading of TMPyP (molar ratio $TMPyP/SO_3^-$ = 7.5 × 10^{-3}) led to longer average fluorescence lifetimes similar to the fluorescence spectroscopy experiments (Figure 6d–f). The polymodal fluorescence lifetime distribution was due to heterogeneity of the materials (see the Supporting Information, Figures S2 and S3). Fluorescence lifetimes below 5 ns were observed for TMPyP molecules bound to thin nanofibers (with diameter up to 400 nm). The TMPyP molecules with longer average fluorescence lifetimes were located preferentially on thicker nanofibers and large irregularities (micrometer size). The prolongation of the fluorescence lifetimes showed that the TMPyP molecules were located in an environment that was less polar than water.[24] This trend may be due to the multiple

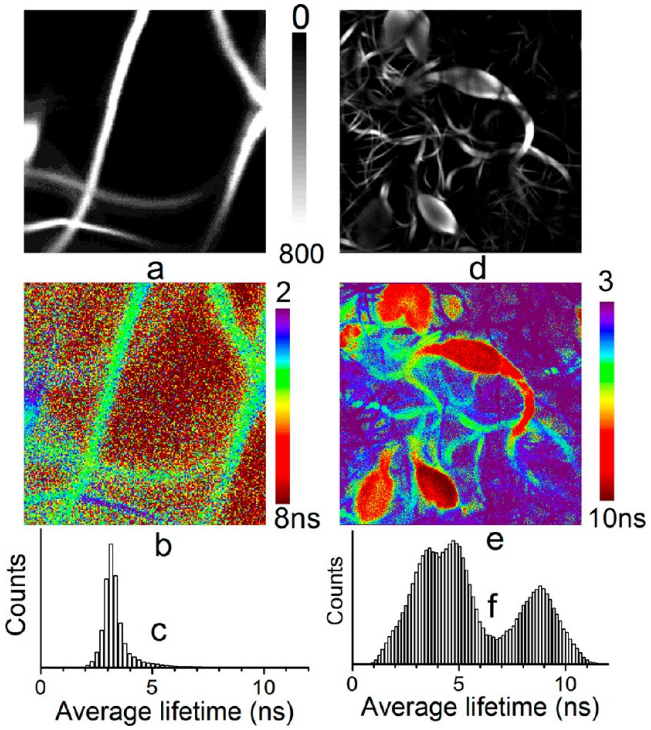

Figure 6. FLIM analysis of the TMPyP nanofiber materials: (a) intensity and (b) lifetime images (20 × 20 μm) and (c) the histogram of average lifetimes at the high loading ($TMPyP/SO_3^-$ = 0.93); (d) intensity and (e) lifetime images (50 × 50 μm) and (f) the histogram of average lifetimes of TMPyP at irregularities at the medium loading ($TMPyP/SO_3^-$ = 7.5 × 10^{-3}).

binding of TMPyP molecules to two or more sulfonated groups in a manner that is similar to the binding of TMPyP on anionic clay surfaces.[29] This adsorption flattens the molecules and suppresses self-quenching by adjacent molecules.[29,30] Spatially resolved fluorescence decay curves are presented in the Supporting Information (Figures S5 and S6).

Triplet State of TMPyP. The kinetics of the TMPyP triplet states of the TMPyP nanofiber materials were studied with nanosecond laser flash photolysis in both reflection and transmission modes. The typical decay curve at the low loading of TMPyP deviated from single-exponential kinetics (Figure 7a). In a double-exponential model, the fraction of TMPyP triplets with a lifetime of approximately 5−9 μs was quenched by oxygen. An estimated Stern−Volmer rate constant of 1.5 × 10^8 M^{-1} s^{-1} indicated the formation of $O_2(^1\Delta_g)$. The rest of the TMPyP triplets was not quenched by oxygen. The amount of unquenched TMPyP triplets increased with the loading of TMPyP. At high loading levels, the predominant single-exponential kinetics with a lifetime of approximately 500 μs was observed (Figure 7a).

Singlet Oxygen $O_2(^1\Delta_g)$ and Singlet Oxygen-Sensitized Delayed Fluorescence (SODF). The formation of $O_2(^1\Delta_g)$ upon excitation to the Soret band of TMPyP was confirmed by steady-state phosphorescence spectroscopy in the NIR region for both dry and wet samples of the TMPyP nanofiber materials. The spectra included a characteristic band of $O_2(^1\Delta_g)$ at 1269 nm (Figure 7b).

Time-resolved phosphorescence of $O_2(^1\Delta_g)$ was measured with the nanofiber material immersed in D_2O, where the lifetime of $O_2(^1\Delta_g)$ is about twenty times higher than in H_2O.[31] The TMPyP nanofiber material scattered excitation light more effectively than the nanofiber materials doped by porphyrins used in previous studies.[6,14] In addition, the intensity of the signals was lower. Both effects influenced the accuracy and reproducibility of measurements, and the noisy signals did not allow the calculation of the $O_2(^1\Delta_g)$ lifetimes with good precision (Figure 7c).

We also measured SODF signals produced by the materials immersed in water (Figure 7d). SODF originates from the repopulation of singlet excited states of TMPyP by energy

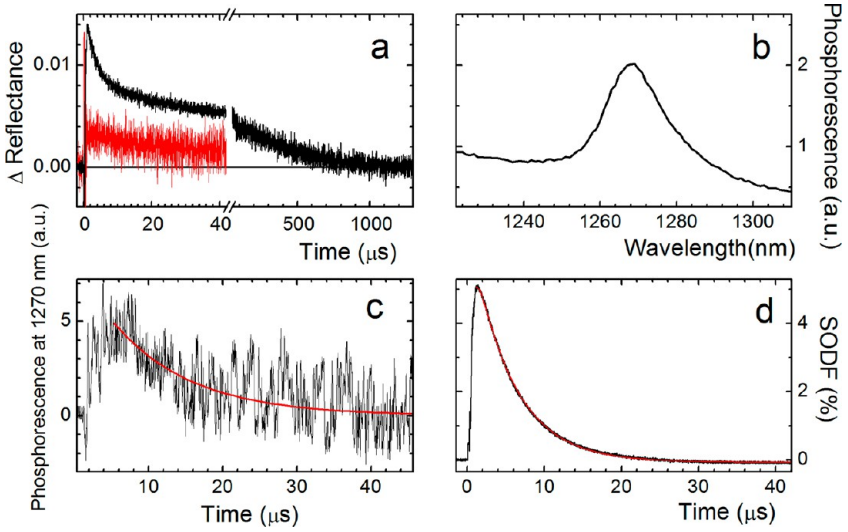

Figure 7. Photophysics of the TMPyP nanofiber materials: (a) Time-resolved transient absorption of the TMPyP triplet states at the low ($TMPyP/SO_3^-$ = 2.5 × 10^{-3}, black line) and high loadings ($TMPyP/SO_3^-$ = 0.93, red line) of TMPyP. The traces were recorded at 480 nm following 308 nm pulsed laser excitation and were measured by diffuse reflectance laser flash photolysis in air-saturated H_2O. (b) Phosphorescence band of $O_2(^1\Delta_g)$ with a maximum at 1269 nm observed after excitation of the TMPyP nanofiber material ($TMPyP/SO_3^-$ = 0.93) at 430 nm; (c) corresponding time-resolved phosphorescence of $O_2(^1\Delta_g)$ fitted by a single-exponential function (red line); and (d) the corresponding SODF signal at 670 nm expressed in percentage of fluorescence amplitude). Both signals (c, d) were calculated as differences between the signals in oxygen- and argon-saturated D_2O, excitation wavelength was 425 nm.

dx.doi.org/10.1021/am4004057 | ACS Appl. Mater. Interfaces 2013, 5, 3776−3783

transfer between the triplet states and $O_2(^1\Delta_g)$. We found strong SODF signals for all three TMPyP loadings. The analysis of the SODF kinetics[32] gave the lifetime of $O_2(^1\Delta_g)$, τ_Δ, below 1 μs (see the Supporting Information, Table S1, for details), which is shorter than the lifetime of $O_2(^1\Delta_g)$ in H_2O (τ_Δ = 3.5 μs)[33] and suggests that $O_2(^1\Delta_g)$ produced at the nanofiber surfaces interacts with the polymer backbones and/or surrounding porphyrin molecules. Assuming the oxygen diffusion coefficient in H_2O ($D = 2 \times 10^{-5}$ cm^2 s^{-1}),[34] the calculated mean radial diffusion length, $l_r = (6D\tau_\Delta)^{1/2}$, traveled by $O_2(^1\Delta_g)$ was approximately 10 nm for a typical value of τ_Δ = 0.7 μs obtained from SODF measurements.

Singlet oxygen $O_2(^1\Delta_g)$ is generated on the nanofiber surfaces in a close proximity to a target species that can be efficiently photooxidized. In contrast, the hydrophobic surface of the materials with porphyrins immobilized inside the polystyrene fibers prevents a close contact between $O_2(^1\Delta_g)$ and a hydrophilic target species in the water environment.[6,7] This disadvantage is partially compensated with a longer lifetime of $O_2(^1\Delta_g)$ in the nanofibers (τ_Δ = 13.5 μs).[7] Singlet oxygen generated inside the nanofibers diffuses to the water environment (τ_Δ = 3.5 μs), where it can oxidize a target species for a longer time than $O_2(^1\Delta_g)$ generated by the TMPyP nanofiber material with τ_Δ of 0.7 μs.

We also used SODF for the imaging of $O_2(^1\Delta_g)$ by FLIM according to the procedure described in our previous paper.[32] We found that very low intensity SODF images reproduced the prompt fluorescence images (see the Supporting Information, Figure S4).

Adsorption and Photo-oxidation of Compounds. Adsorption and photooxidation of individual species dissolved in water were detected by AAS (Pb^{2+}) or UV/vis spectroscopy (I^-, I_3^-) of the water phase. For these experiments, the TMPyP nanofiber material with the low porphyrin loading (TMPyP/SO_3^- ratio of 2.5×10^{-3}) was selected because the majority of its $-SO_3^-$ groups were free to attract positively charged species, e.g., cations of heavy metals.

As expected, we observed fast adsorption of Pb^{2+} ions on nanofiber surfaces after immersing the sulfonated (Figure 8a)

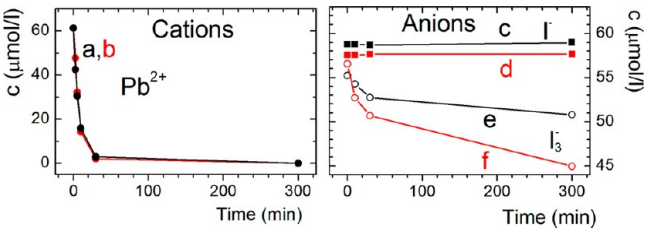

Figure 8. Adsorption isotherms: (a) Pb^{2+}, (c) I^-, or (e) I_3^- on the sulfonated nanofiber material; (b) Pb^{2+}, (d) I^-, and (f) I_3^- on the TMPyP nanofiber material (TMPyP/SO_3^- = 2.5×10^{-3}). *c* designates concentration of individual species in the water phase (3 mL) after immersion of the nanofiber materials (3 cm^2) in the dark.

and the TMPyP nanofiber materials (Figure 8b) in solutions of Pb^{2+}. The isotherms were not affected by the low TMPyP loading because no more than 1% of the sulfonic groups were compensated by TMPyP. In contrast to cationic species, anions such as I^- were not adsorbed on any of these materials because of electrostatic repulsions (Figure 8c, d). Only small amounts of triiodide anions (I_3^-) adsorbed on the TMPyP nanofiber materials because of their greater polarizability, and ion pairing between some uncompensated *N*-methylpyridinium groups of TMPyP and I_3^- (Figure 8e, f).[35]

Depending on their charge and polarizability, the photooxidation products may be adsorbed on the fiber surfaces or released into the surrounding environment. We studied the generation of I_3^-, which is a product of the photooxidation of I^- by $O_2(^1\Delta_g)$ sensitized by TMPyP (see the Supporting Information, eqs S2–S5).[19] Although I^- was not adsorbed on the surface of TMPyP nanofiber materials (Figure 8d), slight adsorption of I_3^- was observed (Figure 8f).

Continuous irradiation of the TMPyP nanofiber materials in aerated aqueous solutions of I^- was accompanied by a linear increase of the I_3^- concentration in the water phase (Figure 9 a-

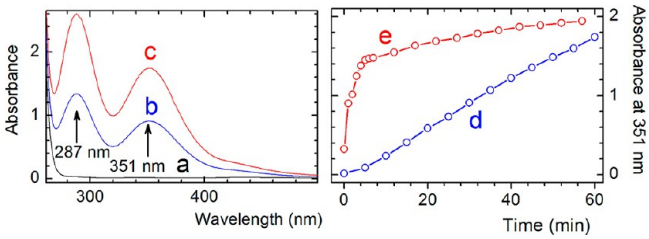

Figure 9. Absorption spectra of an air-saturated aqueous solution of 0.05 M I^- (3 mL) containing a piece of TMPyP nanofiber material (3 cm^2, TMPyP/SO_3^- = 2.5×10^{-3}) after (a) 0, (b) 30, and (c) 60 min of continuous irradiation, where the arrows indicate changes in the absorption bands. (d) Time dependence of I_3^- absorbance at 351 nm is compared with (e) kinetics of I_3^- formation mediated by 1×10^{-5} M TMPyP aqueous solution.

c). No release of TMPyP from the nanofiber surfaces to the water phase was detected. The TMPyP nanofiber materials, whether in the dark or irradiated in the absence of dissolved oxygen, and the irradiated TMPyP-free materials did not produce any I_3^- because no $O_2(^1\Delta_g)$ was generated. The formation of I_3^- was accelerated in D_2O, where the lifetime of $O_2(^1\Delta_g)$ is longer than in H_2O, and the reaction completely stopped in the presence of a large excess of NaN_3 (~0.01 mol L^{-1}), which is an effective physical quencher of $O_2(^1\Delta_g)$ (see the Supporting Information, Figure S9).

The linear increase in I_3^- concentration mediated with TMPyP nanofiber material (Figure 9d) was in contrast to the nonlinear kinetics of the I_3^- formation in aqueous solution of TMPyP (Figure 9e). In the latter case, the formation of $O_2(^1\Delta_g)$ stopped after reaching a critical concentration of I_3^-, which was necessary for quantitative ion pairing with TMPyP. The ion pair TMPyP-I_3^- is known to undergo extensive aggregation, which is connected with the complete cessation of $O_2(^1\Delta_g)$ formation.[35] The binding of TMPyP to the sulfonated surface evidently prevented the photoinduced aggregation. The ability of the TMPyP nanofiber materials to photogenerate $O_2(^1\Delta_g)$ was also verified using uric acid that is a known acceptor of $O_2(^1\Delta_g)$.[36] The reaction was monitored by the decrease in the uric acid absorbance at 291 nm (see the Supporting Information, Figure S10).

Antibacterial Activity. The antibacterial properties of the TMPyP nanofiber material induced by light irradiation were demonstrated for the DH5α *E. coli* strain with the pGEM11Z plasmid. Figure 10 displays samples of nanofiber materials treated with bacterial colonies of *E. coli* (Supporting Information, Figure S11). These bacterial colonies produce β-galactosidase, which cleaves the X-Gal substrate into an indolyl dye that forms a visible blue-green color. Strong inhibition of

dx.doi.org/10.1021/am4004057 | ACS Appl. Mater. Interfaces 2013, 5, 3776–3783

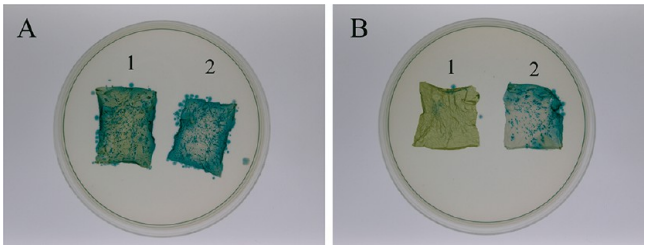

Figure 10. Agar plates with pieces of the TMPyP nanofiber material ($TMPyP/SO_3^- = 2.5 \times 10^{-3}$, sample 1) or sulfonated material without TMPyP (sample 2) when (B) irradiated with a 400 W solar simulator for 2 min or (A) stored in the dark. The samples were inoculated with the *E. coli* strain DH5α (blue-green spots) before irradiation.

bacterial colony growth was observed on the surface of the TMPyP nanofiber material ($TMPyP/SO_3^- = 2.5 \times 10^{-3}$) after 2 min of irradiation with visible light from a solar simulator (Figure 10 B1), whereas the colonies grew normally on agar outside of the nanofiber material. The bacterial growth was not inhibited by the nanofiber materials with and without TMPyP that were stored in the dark (Figure 10 A), which is in agreement with the $O_2(^1\Delta_g)$ sensitizing mechanism. In this case, the bacterial colonies grew everywhere, including on the surface of the nanofiber material. The sulfonated nanofiber materials without TMPyP did not exhibit any antibacterial properties upon irradiation with light (Figure 10 B2).

Because of their antibacterial properties, these TMPyP nanofiber materials are a suitable alternative for use in topical antibiotics and antiseptics and could be effective for use in in vivo experiments. Similar to nanofiber materials with encapsulated porphyrins,[13] only superficial effects can be expected in comparison to standard antiseptic treatment, which suggests that the antibacterial activity of the materials will not interfere with normal healing processes.

4. CONCLUSION

The electrospun polystyrene nanofiber materials sulfonated with chlorosulfonic acid are ideal substrates for the adsorption of porphyrin assemblies that can effectively generate singlet oxygen. The combination of the electrospinning technique and electrostatic assembly allows us to take advantage of the highly specific surface area, easy exposure of the porphyrin molecules to light and oxygen, flexibility, lightweight, and high porosity of the nanofiber materials while simultaneously providing versatile properties that can be fine-tuned by varying the porphyrin/-SO_3^- ratio.

The sulfonated electrospun material with externally bound porphyrin molecules consists of a polystyrene core and a shell that is chemically tailored for applications, including the rapid, selective adsorption of cationic species, such as heavy metal cation contaminants or organic pollutants, and the killing of bacteria by singlet oxygen. The shell is capable of performing multiple tasks, e.g., photodisinfection, decontamination, and separation using the same material.

Despite that the TMPyP nanofiber materials generate $O_2(^1\Delta_g)$ with lower lifetimes ($\tau_\Delta \approx 0.7$ μs) than the previously reported nanofiber material with porphyrin immobilized inside the polystyrene nanofibers ($\tau_\Delta = 13.5$ μs), both materials exhibited a comparable photooxidation activity in aqueous media. The reasons can consist in a good contact of the hydrophilic surface of the TMPyP nanofiber materials with biological targets or polar chemical substrates and in the fact that $O_2(^1\Delta_g)$ does not diffuse through the polymer bulk to aqueous media.

■ ASSOCIATED CONTENT

Supporting Information

FLIM data, fluorescence kinetics and spectra, analysis of SODF data, additional adsorption and photooxidation experiments, mechanism of I^- photooxidation, image of bacteria on nanofiber surface. This material is available free of charge via the Internet at http://pubs.acs.org/.

■ AUTHOR INFORMATION

Corresponding Author

*E-mail: pavel.kubat@jh-inst.cas.cz (P.K.); mosinger@natur.cuni.cz (J. M.).

Notes

The authors declare no competing financial interest.

■ ACKNOWLEDGMENTS

This work was supported by the Czech Science Foundation (Projects 13-12496S and P208/10/1678) and by the Ministry of Education, Youth and Sports of the Czech Republic (MSM 0021620857). The authors thank Dr. Lukáš Plíštil for preparing the nanofiber materials using the electrospinning technique. J.S. acknowledges the Czech Science Foundation (Project P208/12/G016) for support of FLIM measurements.

■ REFERENCES

(1) Maisch, T.; Baier, J.; Franz, B.; Maier, M.; Landthaler, M.; Szeimies, R. M.; Baumler, W. *Proc. Natl. Acad. Sci. U.S.A.* **2007**, *104*, 7223−7228.
(2) Hamblin, M. R.; Hasan, T. *Photochem. Photobiol. Sci.* **2004**, *3*, 436−450.
(3) Allison, R. R.; Sibata, C. H. *Photodiagn. Photodyn. Ther.* **2010**, *7*, 61−75.
(4) Cló, E.; Snyder, J. W.; Ogilby, P. R.; Gothelf, K. V. *ChemBioChem* **2007**, *8*, 475−481.
(5) Lang, K.; Mosinger, J.; Wagnerová, D. M. *Coord. Chem. Rev.* **2004**, *248*, 321−350.
(6) Mosinger, J.; Jirsák, O.; Kubát, P.; Lang, K.; Mosinger, B. *J. Mater. Chem.* **2007**, *17*, 164−166.
(7) Jesenská, S.; Plíštil, L.; Kubát, P.; Lang, K.; Brožová, L.; Popelka, Š.; Szatmáry, L.; Mosinger, J. *J. Biomed. Mater. Res. A* **2011**, *99A*, 676−683.
(8) Lhotáková, Y.; Plíštil, L.; Morávková, A.; Kubát, P.; Lang, K.; Forstová, J.; Mosinger, J. *PLoS ONE* **2012**, *7*, e49226.
(9) Reneker, D. H.; Chun, I. *Nanotechnology* **1996**, *7*, 216−223.
(10) Greiner, A.; Wendorff, J. H. *Angew. Chem., Int. Ed.* **2007**, *46*, 5670−5703.
(11) Pitsillides, C. M.; Joe, E. K.; Wei, X.; Anderson, R. R.; Lin, C. P. *Biophys. J.* **2003**, *84*, 4023−4032.
(12) Gracanin, M.; Hawkins, C. L.; Pattison, D. I.; Davies, M. J. *Free Radical Biol. Med.* **2009**, *47*, 92−102.
(13) Arenbergerová, M.; Arenberger, P.; Bednář, M.; Kubát, P.; Mosinger, J. *Exp. Dermatol.* **2012**, *21*, 619−624.
(14) Mosinger, J.; Lang, K.; Plíštil, L.; Jesenská, S.; Hostomský, J.; Zelinger, Z.; Kubát, P. *Langmuir* **2010**, *26*, 10050−10056.
(15) Arai, T.; Tanaka, M.; Kawakami, H. *ACS Appl. Mater. Interfaces* **2012**, *4*, 5453−5457.
(16) Wilkinson, F.; Helman, W. P.; Ross, A. B. *J. Phys. Chem. Ref. Data* **1993**, *22*, 113−262.
(17) Lee, J.; Kang, S.; Lee, Y.; Nam, J. *Polymer Bull.* **2010**, *64*, 717−725.
(18) Šlouf, M.; Lapčíková, M.; Štěpánek, M. *Eur. Polym. J.* **2011**, *47*, 1273−1278.
(19) Mosinger, J.; Mosinger, B. *Experientia* **1995**, *51*, 106−109.

(20) Subramanian, C.; Giotto, M.; Weiss, R. A.; Shaw, M. T. *Macromolecules* **2012**, *45*, 3104−3111.
(21) Atorngitjawat, P.; Runt, J. *Macromolecules* **2007**, *40*, 991−996.
(22) de Miguel, G.; Pérez-Morales, M.; Martín-Romero, M. T.; Muñoz, E.; Richardson, T. H.; Camacho, L. *Langmuir* **2007**, *23*, 3794−3801.
(23) Rywkin, S.; Hosten, C. M.; Lombardi, J. R.; Birke, R. L. *Langmuir* **2002**, *18*, 5869−5880.
(24) Gonçalves, P. J.; Franzen, P. L.; Correa, D. S.; Almeida, L. M.; Takara, M.; Ito, A. S.; Zílio, S. C.; Borissevitch, I. E. *Spectrochim. Acta A* **2011**, *79*, 1532−1539.
(25) Paulo, P. M. R.; Costa, S. M. B. *J. Phys. Chem. B* **2005**, *109*, 13928−13940.
(26) Vergeldt, F. J.; Koehorst, R. B. M.; van Hoek, A.; Schaafsma, T. J. *J. Phys. Chem. A* **1995**, *99*, 4397−4405.
(27) Kubát, P.; Sebera, J.; Záliš, S.; Langmaier, J.; Fuciman, M.; Polivka, T.; Lang, K. *Phys. Chem. Chem. Phys.* **2011**, *13*, 6947−6954.
(28) Ruthard, C.; Maskos, M.; Kolb, U.; Gröhn, F. *J. Phys. Chem. B* **2011**, *115*, 5716−5729.
(29) Ishida, Y.; Shimada, T.; Masui, D.; Tachibana, H.; Inoue, H.; Takagi, S. *J. Am. Chem. Soc.* **2011**, *133*, 14280−14286.
(30) Ishida, Y.; Masui, D.; Shimada, T.; Tachibana, H.; Inoue, H.; Takagi, S. *J. Phys. Chem. C* **2012**, *116*, 7879−7885.
(31) Wilkinson, F.; Helman, W. P.; Ross, A. B. *J. Phys. Chem. Ref. Data* **1995**, *24*, 663−1021.
(32) Mosinger, J.; Lang, K.; Hostomský, J.; Franc, J.; Sýkora, J.; Hof, M.; Kubát, P. *J. Phys. Chem. B* **2010**, *114*, 15773−15779.
(33) Poulsen, T. D.; Ogilby, P. R.; Mikkelsen, K. V. *J. Phys. Chem. A* **1998**, *102*, 9829−9832.
(34) Tsushima, M.; Tokuda, K.; Ohsaka, T. *Anal. Chem.* **1994**, *66*, 4551−4556.
(35) Mosinger, J.; Janošková, M.; Lang, K.; Kubát, P. *J. Photochem. Photobiol. A* **2006**, *181*, 283−289.
(36) Abós, P.; Artigas, C.; Bertolotti, S.; Braslavsky, S. E.; Fors, P.; Lang, K.; Nonell, S.; Rodríguez, F. J.; Sesé, M. L.; Trull, F. R. *J. Photochem. Photobiol. B* **1997**, *41*, 53−59.